



HAL
open science

Pyrite sulfur isotopes reveal glacial–interglacial environmental changes

Virgil Pasquier, Pierre Sansjofre, Marina Rabineau, Sidonie Révillon, Jennifer Houghton, David A. Fike

► **To cite this version:**

Virgil Pasquier, Pierre Sansjofre, Marina Rabineau, Sidonie Révillon, Jennifer Houghton, et al.. Pyrite sulfur isotopes reveal glacial–interglacial environmental changes. *Proceedings of the National Academy of Sciences of the United States of America*, 2017, 114 (23), pp.5941-5945. 10.1073/pnas.1618245114 . hal-01592589

HAL Id: hal-01592589

<https://hal.univ-brest.fr/hal-01592589>

Submitted on 25 Sep 2017

HAL is a multi-disciplinary open access archive for the deposit and dissemination of scientific research documents, whether they are published or not. The documents may come from teaching and research institutions in France or abroad, or from public or private research centers.

L'archive ouverte pluridisciplinaire **HAL**, est destinée au dépôt et à la diffusion de documents scientifiques de niveau recherche, publiés ou non, émanant des établissements d'enseignement et de recherche français ou étrangers, des laboratoires publics ou privés.

25 **Abstract:**

26 The sulfur biogeochemical cycle plays a key role in regulating Earth's surface redox
27 through diverse abiotic and biological reactions that have distinctive stable isotopic
28 fractionations. As such, variations in the sulfur isotopic composition ($\delta^{34}\text{S}$) of sedimentary sulfate
29 and sulphide phases over Earth history can be used to infer substantive changes to the Earth's
30 surface environment, including the rise of atmospheric oxygen. Such inferences assume that
31 individual $\delta^{34}\text{S}$ records reflect temporal changes in the global sulfur cycle; this assumption may
32 be well grounded for sulfate-bearing minerals, but is less well established for pyrite-based
33 records. Here, we investigate alternative controls on the sedimentary sulfur isotopic composition
34 of marine pyrite by examining a 300 m drill core of Mediterranean sediments deposited over the
35 past 500,000 years and spanning the last five glacial-interglacial periods. Because this interval is
36 far shorter than the residence time of marine sulfate, any change in the $\delta^{34}\text{S}_{\text{pyr}}$ record necessarily
37 corresponds to local environmental changes. The stratigraphic variations ($>76.8\text{‰}$) in the
38 isotopic data reported here are among the largest ever observed in pyrite, and are in phase with
39 glacial-interglacial sea level and temperature changes. In this case, the dominant control appears
40 to be glacial-interglacial variations in sedimentation rates. These results suggest that there exist
41 important but previously overlooked depositional controls on sedimentary sulfur isotope records,
42 especially associated with intervals of substantial sea level change. This work provides important
43 perspective on the origin of variability in such records and suggests novel paleoenvironmental
44 information can be derived from pyrite $\delta^{34}\text{S}$ records.

45

46

47 **Significant Statement**

48 Sulfate is a major oxidant in the global ocean with a long residence time (13 Myr). As such,
49 changes in sulfur isotopes ratio ($^{34}\text{S}/^{32}\text{S}$) of marine sulfur phases are often attributed to global
50 biogeochemical perturbations. Sediments collected on the shelf of the Gulf of Lion, revealed
51 remarkable sulfur isotopic fluctuations in sedimentary pyrite over the last 500,000 years, ranging
52 between -44.0‰ and 32.3‰. We suggest this pattern is related to changes in the local
53 environmental deposition, specifically sedimentation modulating connectivity with the overlying
54 water column and resulting microbial activity. Besides providing new understanding of an
55 important and poorly constrained aspect of past glacial-interglacial transitions, our results are
56 critically important because they question the degree to which changes in sulfur isotopes in pyrite
57 reflect global biogeochemical processes versus local depositional conditions.

58
59

60 \body

61 The sulfur biogeochemical cycle helps regulate Earth's surface redox conditions through a
62 variety of abiotic and biological reactions (1). These diverse reactions are often associated with
63 distinctive stable isotopic fractionations of sulfur species (2, 3). As such, changes in the sulfur
64 isotopic composition ($\delta^{34}\text{S}$) of sedimentary phases over Earth history are often used to infer
65 substantive changes to the Earth's surface environment, including the rise of atmospheric oxygen,
66 the oxygenation of the oceans, and episodes of metazoan evolution and mass extinction (2-6).
67 Much of past efforts to reconstruct the ancient sulfur cycle has used sulfate evaporite minerals
68 (gypsum and anhydrite), barium-sulfate (barite), or carbonate-associated sulfate (i.e. sulfate
69 bound into carbonate lattice, CAS) – all proxies that are generally thought to accurately reflect
70 the $\delta^{34}\text{S}$ composition seawater sulfate (2, 7). Additional constraints on ancient biogeochemical
71 cycling have been placed through the analysis of $\delta^{34}\text{S}$ records from sedimentary pyrites, either in
72 parallel with direct proxies for sulfate (4, 6, 8, 9), or on their own (10-13). Inferences about past
73 biogeochemical cycling are based on the assumption that the $\delta^{34}\text{S}$ records reflect the isotopic
74 composition of seawater sulfate and, further, that changes in these values indicate large-scale
75 temporal changes in the global sulfur cycle. However, a subset of records of sulfur cycling from
76 certain intervals on Earth have shown substantial spatial and stratigraphic variability that is not
77 easily reconciled with them reflecting the behavior of the global sulfur cycle (e.g., 14). Rather, it

78 has been suggested that some $\delta^{34}\text{S}$ records have the potential to be impacted by local depositional
79 conditions (2) – and further that these records may provide new insights into paleo-environmental
80 conditions. This intriguing idea has, however, not yet been appropriately tested.

81 Here we examine the sulfur isotopic record preserved in pyrite ($\delta^{34}\text{S}_{\text{pyr}}$) from sediments
82 from the Gulf of Lion deposited over the last 500,000 years associated with the last five glacial-
83 interglacial transitions. Gulf of Lion is located in the North-Western Mediterranean basin and is
84 characterized by a wide continental shelf (70 km) that was sub-aerially exposed during glacial
85 periods over the Late Quaternary (15, 16). This study is based on borehole PRGL 1-4 (Fig. 1),
86 drilled in the framework of the EU PROMESS project
87 (<http://www.pangaea.de/Projects/PROMESS1/>), which sampled a 300 m long continuous record
88 of the Bourcart and Herault canyons' interfluvial sediment sequence on the upper slope of the Gulf
89 of Lion (Fig. 1). The water depth of the core (298 m) ensures continued deposition under well
90 oxygenated conditions during glacial and interglacial periods with sedimentation rates that enable
91 high-resolution records and where the changing proximity to the continental shelf results in
92 variable detrital input. Given these characteristics, this drill core represents a record of glacial-
93 interglacial deposition that is uniquely positioned to assess the environmental dependence of
94 $\delta^{34}\text{S}_{\text{pyr}}$ signatures in marine sediments.

95

96 **Results and Discussion**

97 A total of 131 pyrite sulfur isotopes analyses have been performed along the 300 m
98 PRGL1-4 core, spanning the last 5 glacial-interglacial transitions (see Supporting Information
99 Fig. 1). Throughout the core, pyrite shows extreme variations in $\delta^{34}\text{S}$ from -44.0‰ to 32.3‰,
100 while pyrite contents vary between 0.02 and 1.69 weight %. No clear trend was observed
101 between $\delta^{34}\text{S}_{\text{pyr}}$ and the pyrite content, nor between $\delta^{34}\text{S}_{\text{pyr}}$ and the iron content (see Supporting
102 Informations S1 and S2). Complementary analysis of organic carbon isotopes ($\delta^{13}\text{C}_{\text{org}}$) was
103 conducted and these values vary between -25.3‰ and -21.8‰ with no clear trends between
104 $\delta^{13}\text{C}_{\text{org}}$ and total organic carbon (TOC) contents, which vary between 0.35% and 0.84%.

105 A clear distinction in pyrite $\delta^{34}\text{S}_{\text{pyr}}$ values is observed between glacial and interglacial
106 periods (Fig. 2) as deduced from the oxygen isotope curve obtained from planktonic foraminifera
107 [*G. bulloides*] and the associated updated age model published on the same core (17). Distinctly
108 different bimodal distributions are observed between glacial (*sensu stricto*, i.e., cold substages)

109 periods with high $\delta^{34}\text{S}$ values and high isotopic variability (average $\delta^{34}\text{S} = -15.2\text{‰} \pm 9.0\text{‰}$, $n =$
110 46) and the interglacial (*sensu stricto*, i.e., warm substages) periods characterized by low $\delta^{34}\text{S}$
111 and low isotopic variability (average $\delta^{34}\text{S} = -41.6\text{‰} \pm 2.2\text{‰}$, $n = 19$; Fig. 2). The increased
112 variability observed during glacial times provides insights into the suite of process and their
113 inherent temporal fluctuations that are likely to regulate the observed changes in $\delta^{34}\text{S}_{\text{pyr}}$.
114 Specifically, the lowered sea level during glacial times brought the site of deposition closer to the
115 shore and source of detrital materials. These shallower, more proximal settings are subjected to
116 short-term, stochastic variations in depositional conditions (17), including sediment
117 characteristics (organic carbon loading, sedimentation rates; physical reworking) and benthic
118 ecology (bioturbation, presence of microbial mats) that can impact pyrite formation and eventual
119 $\delta^{34}\text{S}$ composition. Within the glacial and interglacial sediments, the $\delta^{34}\text{S}$ values and variability
120 can be further understood as a function of temperature, as reconstructed from alkenone records
121 (18, 19). For example, warmer intervals during interglacial time are associated with more
122 negative $\delta^{34}\text{S}$ values (Fig. 2).

123 Over the last two glacial-interglacial cycles, where the time reconstruction is best
124 constrained, pyrite $\delta^{34}\text{S}$ values in PRGL1-4 are modulated by and track depositional conditions
125 across glacial-interglacial cycles (Fig. 3). During glacial times, higher $\delta^{34}\text{S}_{\text{pyr}}$ values are
126 associated with lower sea levels, and low $\delta^{13}\text{C}_{\text{org}}$ values, which are often attributed to greater
127 input of terrestrial organic matter (20). Interestingly, because of their increased proximity to
128 shore, glacial deposits are also associated with increased sedimentation rates (21) and are
129 characterized by decreased porosity intervals (see Supporting Information Fig. 2). In such
130 nearshore environments, the rapid sediment burial ensures that a higher concentration of labile
131 organic matter (supported by our TOC values) gets into the sediment without undergoing aerobic
132 respiration. As such, a larger fraction of more easily metamobilizable (i.e., less degraded by oxic
133 processes) organic matter is available for sulfate reduction (22).

134 In contrast, decreased and less variable $\delta^{34}\text{S}_{\text{pyr}}$ values are associated with the transition into
135 and during interglacial times. These are associated with warmer temperatures and higher sea
136 levels, as well as increased $\delta^{13}\text{C}_{\text{org}}$ values, indicative of increased marine input (23). Sediments
137 deposited during interglacial periods are also associated with lower sedimentation rates (because
138 of landward migration of the shoreline) and increased foraminiferal abundance, resulting in
139 intervals of higher porosity (21; see Supplementary Fig. 2). As sedimentation rates decrease,

140 organic matter spends more time in the zone of aerobic respiration. Therefore, less (and less
141 reactive) organic matter remains for sulfate-reducing bacteria under these conditions.

142 Stratigraphic variations in pyrite $\delta^{34}\text{S}$ are often interpreted to reflect changes in the global
143 sulfur biogeochemical cycle, such as intervals of enhanced pyrite burial or variations in the
144 marine sulfate reservoir (9, 24). However, in this case, these strata were deposited over an
145 interval of 500 kyr, much less than the residence time (13 Myr; ref. 25) of sulfate in the modern
146 ocean. While these sediments were deposited in the Gulf of Lion, the Mediterranean Sea
147 maintained connectivity with the global ocean and retained marine sulfate abundances and
148 isotopic compositions during glacial-interglacial periods, based on both the abundance and
149 isotopic composition of sulfate porewater profiles (26) and the continuous sea water infill of
150 Mediterranean Sea by Atlantic water through the Gibraltar Strait since ~4.4 Ma (27, 28). Thus,
151 continued connectivity with the ocean and the short timescale of deposition preclude any
152 substantive change in the parent sulfate reservoir, such as might arise from prolonged variation in
153 the burial flux of pyrite, during deposition of these sediments. How then is this variation in pyrite
154 $\delta^{34}\text{S}$ to be interpreted?

155 Two possible mechanisms present themselves to explain the observed data – both
156 fundamentally driven by glaciation induced environmental changes: one reflecting changes in the
157 inherent metabolic activity of sulfur cycling microbes in the sediments; the other, changes in the
158 connectivity of porewaters to the overlying water column. In the former, isotopic fractionation
159 during microbial sulfur cycling is typically dominated by microbial sulfate reduction (3) and a
160 change in pyrite $\delta^{34}\text{S}$ can result from variations in the rate of cell-specific sulfate reduction
161 (csSRR) in these sediments (29). Specifically, there is a well-documented relationship whereby
162 faster rates of csSRR are associated with decreased isotopic fractionation between the parent
163 sulfate and the produced sulfide (29, 30). Thus, our data could indicate faster csSRR during
164 glacial times, possibly driven by enhanced input of more easily metabolizable organic matter
165 and/or enhanced terrestrial nutrient input (as supported by lower organic carbon isotopic values,
166 see Supplementary Fig. 1). In contrast, slower csSRR would characterize interglacial times
167 associated with more limited (both in abundance and reactivity) organic matter resources and
168 more stable nutrient input.

169 Assuming that pyrite is formed mainly in the pore-water environment, as it is expected
170 under oxygenated (non euxinic) water column (31), an alternative mechanism to explain our data

171 involves a change in the connectivity of sedimentary porewaters where pyrites are forming with
172 the overlying water column (32). Such a change could be the natural result of the increased
173 sedimentation rates and decreased porosity during glacial times (Supplementary Fig. 2), both of
174 which act to more effectively isolate porewaters from ready communication with seawater. This
175 decreased connectivity effectively isolates the local porewater sulfate reservoir, leading to
176 increased porewater $\delta^{34}\text{S}_{\text{SO}_4}$ through ongoing microbial sulfate reduction (32). In turn, this
177 microbial activity naturally leads to an increase in the resulting biogenic $\delta^{34}\text{S}_{\text{H}_2\text{S}}$, which
178 eventually forms pyrite following reaction with available iron. The increased variability in $\delta^{34}\text{S}_{\text{pyr}}$
179 during glacial times can be understood as the natural response to increased short-term
180 fluctuations in depositional conditions that characterize shallower water environments more
181 proximal to the shore. During interglacial times, the return to slower sedimentation rates and
182 higher porosity, driven in part by the admixture of foraminifera (Supplementary Fig. 2), results in
183 enhanced communication between porewater and seawater. In this relatively open system, the
184 constant supply of seawater sulfate results in a stable, low value for porewater $\delta^{34}\text{S}_{\text{SO}_4}$ (and
185 therefore in the resulting $\delta^{34}\text{S}_{\text{pyr}}$) in these intervals. While the relationship between sedimentation
186 rate and $\delta^{34}\text{S}_{\text{pyr}}$ indicates a dominant control by sedimentation (Fig. 4), it should be noted that
187 these two mechanisms are not mutually exclusive. Indeed, all things being equal, increased
188 csSRR will inherently lead to more closed system behavior because it represents enhanced sulfate
189 consumption relative to the diffusive exchange of sulfate. Further, there is a general trend toward
190 increasing rates of sulfate reduction with increasing sedimentation rate (33).

191 The magnitude and directionality of the relationship between water depth and pyrite $\delta^{34}\text{S}$
192 observed here agree with predictions previously made (2) but never rigorously tested and provide
193 a powerful new way to reconstruct paleo-environmental conditions in sedimentary environments,
194 particularly the degree to which sedimentary porefluids may have been in communication with
195 the overlying water column. In addition, the $\delta^{34}\text{S}_{\text{pyr}}$ data presented here also shed light on the
196 possible origins of similar variability in this proxy in deep time.

197

198 **Implication for deep time records:**

199 Many deep time studies make use of direct proxies for seawater sulfate, such as carbonate-
200 associated sulfate (CAS), which are generally thought to reflect marine sulfate with little
201 fractionation (e.g., 7; but see 34). Indeed, studies utilizing direct proxies for seawater sulfate

202 (e.g., 9, 24, 35, 36) can provide powerful insights into ancient biogeochemical conditions. In
203 many cases, however, no direct proxy of seawater sulfate is present and stratigraphic records of
204 $\delta^{34}\text{S}_{\text{pyr}}$ are used to reconstruct global biogeochemical cycling and redox change (e.g., 10-13). In
205 other cases, the isotopic offsets between coeval $\delta^{34}\text{S}$ records from sulfate and pyrite are used to
206 reconstruct marine sulfate levels or the types of microbial metabolism present (e.g., 4, 8). With
207 few exceptions (e.g., 6), these $\delta^{34}\text{S}_{\text{pyr}}$ records are not interpreted in the context of local
208 depositional or facies change.

209 Interestingly, many of the reports showing positive $\delta^{34}\text{S}_{\text{pyr}}$ excursions in the rock record are
210 also associated with shallowing-upwards depositional sequences formed during sea level
211 lowstands. The present study is particularly relevant for considering the ~10-30‰ positive
212 excursions in $\delta^{34}\text{S}_{\text{pyr}}$ that are associated with the initiation and termination of the end-Ordovician
213 Hirnantian glaciation and mass extinction (e.g., 6, 10, 11, 6, 12, 13). Depositional environments at
214 this time experienced a magnitude (~100 m) and timescale ($\sim 10^5$ yr) of sea level change that
215 would have been comparable to those influencing the Pleistocene sediments of the Gulf of Lion.
216 Our data suggest that rather than reflecting a change in the global sulfur cycle, these $\delta^{34}\text{S}_{\text{pyr}}$
217 excursions could also be explained by local changes in depositional conditions, particularly
218 changes in sedimentation that modulate connectivity with the overlying water column (e.g. Fig.
219 4). In this scenario, it is local sedimentological changes that impact how records of sulfur cycling
220 get preserved in sedimentary records. The temporal coincidence of the Hirnantian $\delta^{34}\text{S}_{\text{pyr}}$
221 excursions, found in sections around the world associated with the end Ordovician glaciation,
222 would then be the result of synchronous local changes in environmental conditions in basins
223 around the world, changes driven globally by sea level fluctuations during the onset and
224 termination of the Hirnantian glaciation. Local environmental controls could be relevant for
225 explaining other stratigraphic $\delta^{34}\text{S}_{\text{pyr}}$ excursions in Earth history, particularly those associated
226 with changing depositional facies and lacking a direct proxy for the marine sulfate reservoir (e.g.,
227 37-39). As such, the data presented here show that pyrite $\delta^{34}\text{S}$ can be a valuable new proxy for
228 reconstructing local paleoenvironmental and sedimentological conditions throughout Earth
229 history.

230

231 **Materials and Methods:**

232 *Pyrite Sulfur ($\delta^{34}\text{S}_{\text{pyrite}}$ and S content)*

233 Pyrite sulfur from the samples was extracted using the chromium reduction method (40-
234 42). This method allows a recovering of all reduced inorganic sulfur present in sedimentary
235 samples (pyrite, element sulfur and iron monosulfide phases). During extraction, samples were
236 reacted with ~25 mL of 1M reduced chromium chloride (CrCl_2) solution and 25 mL of 6N HCl
237 for four hours in a specialized extraction line under a Nitrogen atmosphere. The liberated
238 hydrogen sulfide was reacted in a silver nitrate (0.1M) trap, recovering the sulfide as Ag_2S ;
239 reproducibility was under 5% for repeated analyse. Residual Ag_2S were rinsed three times using
240 Mili-Q water, centrifuged then the dried until complete dryness. The Ag_2S powders were
241 homogenized prior to being analysed, then 450 μg was loaded into tin capsules with excess V_2O_5 .
242 The Ag_2S was analysed measuring $^{34}\text{S}/^{32}\text{S}$ ratio following online combustion with a Thermo
243 Delta V Plus coupled with a Costech ECS 4010 Elemental Analyser at Washington University in
244 St Louis. Pyrite sulfur composition are expressed in standard delta notation as per mil (‰)
245 deviations from Vienna Canyon Diablo Troilite (VCDT) with an analytical error of <0.5‰.

246
247 *Organic carbon analyses (δ^3C_{org} and TOC)*

248 Prior to Organic carbon and Nitrogen analyses, the carbonated fraction was removed from
249 bulk samples using excess 1.5 HCl digestion during 48h. During digestion centrifuge tube were
250 placed in ultrasonic bath to increase the mechanical separation of clay and calcium carbonates.
251 After total dissolution residues were washed three times with distilled water, centrifuged then
252 dried at 50°C. The residual powders were homogenized and prior to analyses 30 mg were loaded
253 into tin capsule. Analyses were performed using an Elemental Analyser (EA, Flash 2000 -
254 ThermoScientific) coupled to an isotope ratio mass spectrometer (Delta V+ Thermo Scientific
255 EA-IRMS) at the Pôle de Spectométrie Océan (PSO, Brest, France). Carbon is given as delta
256 notation as per mil deviation from Pee Dee Belemnite (PDB), with an analytical error of <0.2‰
257 (1σ) for organic carbon isotopes. Total Organic Carbon (TOC) were measured using the Thermal
258 Conductivity Detector (TCD) of the Flash EA 2000, ThermoScientific at PSO, Brest, France.

259
260 **Acknowledgements**

261 This work was supported by the "Laboratoire d'Excellence" LabexMER (ANR-10-LABX-19)
262 and co-funded by a grant from the French government under the program "Investissements
263 d'Avenir", and by a grant from the Regional Council of Brittany. The drilling operation was

264 conducted within the European Commission Project PROMESS (contract EVR1-CT-2002-
265 40024). Engineers of FUGRO-BV and the captain and crew of the Amige drilling vessel *Bavenit*
266 are thanked for their dedication during the cruise. The European Promess shipboard party and
267 colleagues at Ifremer are also thanked for previous contributions of data acquisition and
268 processing. The authors warmly acknowledge C. Liorzou who kindly helped during the analytical
269 preparation of samples, and O. Lebeau for assistance on the EA-IRMS in Brest.

270

271 **References:**

- 272 1. Garrels RM, Lerman A (1981) Phanerozoic cycles of sedimentary carbon and sulfur, pp
273 4652–4656.
- 274 2. Fike DA, Bradley AS, Rose CV (2015) Rethinking the ancient sulfur cycle. *Annual Review*
275 *of Earth and Planetary Sciences* 43. doi:10.1146/annurev-earth-060313-054802.
- 276 3. Canfield DE (2001) Biogeochemistry of sulfur isotopes. *Reviews in Mineralogy and*
277 *Geochemistry* 43(1):607–636.
- 278 4. Fike DA, Grotzinger JP, Pratt LM, Summons RE (2006) Oxidation of the Ediacaran
279 Ocean. *Nature* 444:744–747.
- 280 5. Riccardi AL, Arthur MA, Kump LR (2006) Sulfur isotopic evidence for chemocline
281 upward excursions during the end-Permian mass extinction. *Geochimica et Cosmochimica*
282 *Acta* 70:5740–5752.
- 283 6. Jones DS, Fike DA (2013) Dynamic sulfur and carbon cycling through the end-Ordovician
284 extinction revealed by paired sulfate–pyrite $\delta^{34}\text{S}$. *Earth and Planetary Science Letters*
285 363:144–155.
- 286 7. Kampschulte A, Strauss H (2004) The sulfur isotopic evolution of Phanerozoic seawater
287 based on the analysis of structurally substituted sulfate in carbonates. *Chemical Geology*
288 204:255–286.
- 289 8. Hurtgen MT, Halverson GP, Arthur MA (2006) Sulfur cycling in the aftermath of a 635-
290 Ma snowball glaciation: evidence for a syn-glacial sulfidic deep ocean. *Earth and*
291 *Planetary Science Letters* 245:551–570.
- 292 9. Gill BC, Lyons TW, Young SA, Kump LR, Knoll AH (2011) Geochemical evidence for
293 widespread euxinia in the Later Cambrian ocean. *Nature* 469:80–83.
- 294 10. Yan D, Chen D, Wang Q, Wang J, Wang Z (2009) Carbon and sulfur isotopic anomalies
295 across the Ordovician–Silurian boundary on the Yangtze Platform, South China.
296 *Palaeogeography, Palaeoclimatology, Palaeoecology* 274:32–39.
- 297 11. Zhang T, Shen Y, Zhan R, Shen S, Chen X (2009) Large perturbations of the carbon and

- 298 sulfur cycle associated with the Late Ordovician mass extinction in South China. *Geology*
299 37(4):299–302.
- 300 12. Gorjan P, Kaiho K, Fike DA, Xu C (2012) Carbon-and sulfur-isotope geochemistry of the
301 Hirnantian (Late Ordovician) Wangjiawan (Riverside) section, South China: global
302 correlation and environmental event interpretation. *Palaeogeography, Palaeoclimatology,*
303 *Palaeoecology* 337-338:14–22.
- 304 13. Hammarlund EU, Dahl TW, Harper D (2012) A sulfidic driver for the end-Ordovician
305 mass extinction. *Earth and Planetary Science Letters* 331-332:128–139.
- 306 14. Ries JB, Fike DA, Pratt LM, Lyons TW (2009) Superheavy pyrite ($\delta^{34}\text{S}_{\text{pyr}} > \delta^{34}\text{S}_{\text{SCAS}}$)
307 in the terminal Proterozoic Nama Group, southern Namibia: A consequence of low
308 seawater sulfate at the dawn of animal life. *Geology* 37(8):743–746.
- 309 15. Rabineau M, Berné S, Aslanian D, Olivet JL (2005) Sedimentary sequences in the Gulf of
310 Lion: a record of 100,000 years climatic cycles. *Marine and Petroleum Geology* 22:775–
311 804.
- 312 16. Jouet G, Berné S, Rabineau M, Bassetti MA, Bernier P (2006) Shoreface migrations at the
313 shelf edge and sea-level changes around the Last Glacial Maximum (Gulf of Lions, NW
314 Mediterranean). *Marine Geology* 234:21–42.
- 315 17. Cortina A, Sierro FJ, Gonzalez-Mora B, Asioli A (2011) Impact of climate and sea level
316 changes on the ventilation of intermediate water and benthic foraminifer assemblages in
317 the Gulf of Lions, off South France, during MIS 11 in the northwestern Mediterranean
318 Sea(Gulf of Lions). *Palaeogeography, Palaeoclimatology, Palaeoecology* 309:215–228.
- 319 18. Cortina A, Sierro FJ, Flores JA (2015) The response of SST to insolation and ice sheet
320 variability from MIS 3 to MIS 11 in the northwestern Mediterranean Sea (Gulf of Lions).
321 *Geophysical Research Letters* 42:10366–10374.
- 322 19. Cortina A, Grimalt JO, Martrat B (2016) Anomalous SST warming during MIS 13 in the
323 Gulf of Lions (northwestern Mediterranean Sea). *Organic Geochemistry* 92:16–23.
- 324 20. Lamb AL, Wilson GP, Leng MJ (2006) A review of coastal palaeoclimate and relative sea-
325 level reconstructions using $\delta^{13}\text{C}$ and C/N ratios in organic material. *Earth Science*
326 *Reviews* 75:29–57.
- 327 21. Sierro FJ, Andersen N, Bassetti MA, Berné S (2009) Phase relationship between sea level
328 and abrupt climate change. *Quaternary Science Reviews*:1–15.
- 329 22. Canfield DE (1989) Sulfate reduction and oxic respiration in marine sediments:
330 implications for organic carbon preservation in euxinic environments. *Deep Sea Research*
331 36(1):121–138.
- 332 23. Tesi T, Misericocchi S, Goñi MA, Langone L (2007) Source, transport and fate of terrestrial
333 organic carbon on the western Mediterranean Sea, Gulf of Lions, France. *Marine*

- 334 *Chemistry* 105:101–117.
- 335 24. Owens JD, Gill BC, Jenkyns HC (2013) Sulfur isotopes track the global extent and
336 dynamics of euxinia during Cretaceous Oceanic Anoxic Event 2, pp 18407–18412.
- 337 25. Kah LC, Lyons TW, Frank TD (2004) Low marine sulphate and protracted oxygenation of
338 the Proterozoic biosphere. *Nature* 431:834–838.
- 339 26. Böttcher ME, Bernasconi SM, brumsack H-J (1999) 32. CARBON, SULFUR, AND
340 OXYGEN ISOTOPE GEOCHEMISTRY OF INTERSTITIAL WATERS FROM THE
341 WESTERN MEDITERRANEAN. *Proceedings of Ocean Drillings Program, Scientific*
342 *results* 161:413–421.
- 343 27. Rohling EJ, Foster GL, Grant KM, Marino G, Roberts AP (2014) Sea-level and deep-sea-
344 temperature variability over the past 5.3 million years. *Nature* 504:477–482.
- 345 28. Hernández-Molina FJ, Stow D (2014) Onset of Mediterranean outflow into the North
346 Atlantic. *Science* 344(6189):1244–1250.
- 347 29. Sim MS, Ono S, Donovan K, Templer SP (2011) Effect of electron donors on the
348 fractionation of sulfur isotopes by a marine *Desulfobivrio* sp. *Geochimica et*
349 *Cosmochimica Acta* 75:4244–4259.
- 350 30. Leavitt WD, Halevy I, Bradley AS (2013) Influence of sulfate reduction rates on the
351 Phanerozoic sulfur isotope record, pp 11244–11249.
- 352 31. Censi P, Incarbona A, Oliveri E, Bonomo S, Tranchida G (2010) Yttrium and REE
353 signature recognized in Central Mediterranean Sea (ODP Site 963) during the MIS 6–MIS
354 5 transition. *Palaeogeography, Palaeoclimatology, Palaeoecology* 292(1-2):201–210.
- 355 32. Gomes ML, Hurtgen MT (2013) Sulfur isotope systematics of a euxinic, low-sulfate lake:
356 Evaluating the importance of the reservoir effect in modern and ancient oceans. *Geology*
357 41(6):663–666.
- 358 33. Claypool GE (2004) Ventilation of marine sediments indicated by depth profiles of pore
359 water sulfate and $\delta^{34}\text{S}$. *The Geochemical Society Special Publications* 9:59–65.
- 360 34. Present TM, Paris G, Burke A, Fischer W (2015) Large Carbonate Associated Sulfate
361 isotopic variability between brachiopods, micrite, and other sedimentary components in
362 Late Ordovician strata. *Earth and Planetary Science Letters* 432:187–198.
- 363 35. Fike DA, Grotzinger JP (2008) A paired sulfate–pyrite $\delta^{34}\text{S}$ approach to understanding
364 the evolution of the Ediacaran–Cambrian sulfur cycle. *Geochimica et Cosmochimica Acta*
365 72:2636–2648.
- 366 36. Sansjofre P, Cartigny P, Trindade R (2016) Multiple sulfur isotope evidence for massive
367 oceanic sulfate depletion in the aftermath of Snowball Earth. *Nature Communications* 7.
368 doi:10.1038/ncomms12192.

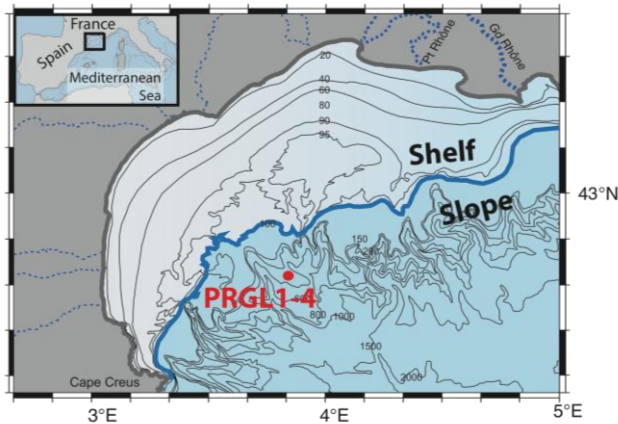
- 369 37. Goldberg T, Strauss H, Guo Q, Liu C (2007) Reconstructing marine redox conditions for
370 the Early Cambrian Yangtze Platform: evidence from biogenic sulphur and organic carbon
371 isotopes. *Palaeogeography, Palaeoclimatology, Palaeoecology* 254:175–193.
- 372 38. Feng LJ, Chu XL, Huang J, Zhang QR, Chang HJ (2010) Reconstruction of paleo-redox
373 conditions and early sulfur cycling during deposition of the Cryogenian Datangpo
374 Formation in South China. *Gondwana Research* 18:632–637.
- 375 39. Parnell J, Boyce AJ, Mark D, Bowden S, Spinks S (2010) Early oxygenation of the
376 terrestrial environment during the Mesoproterozoic. *Nature* 468:290–293.
- 377 40. Canfield DE, Raiswell R, Westrich JT, Reaves CM (1986) The use of chromium reduction
378 in the analysis of reduced inorganic sulfur in sediments and shales. *Chemical Geology*
379 54:149–155.
- 380 41. Tuttle ML, Goldhaber MB, Williamson DL (1986) An analytical scheme for determining
381 forms of sulphur in oil shales and associated rocks. *Talanta* 33(12):953–961.
- 382 42. Burton ED, Sullivan LA, Bush RT, Johnston SG (2008) A simple and inexpensive
383 chromium-reducible sulfur method for acid-sulfate soils. *Applied Geochemistry* 23:2759–
384 2766.
- 385 43. Grant KM, Rohling EJ, Ramsey CB, Cheng H (2014) Sea-level variability over five glacial
386 cycles. *Nature Communications* 5. doi:10.1038/ncomms6076.
- 387 44. Barker S, Knorr G, Edwards RL, Parrenin F (2011) 800,000 years of abrupt climate
388 variability. *Science* 334:347–351.
- 389 45. Railsback LB, Gibbard PL, Head MJ (2015) An optimized scheme of lettered marine
390 isotope substages for the last 1.0 million years, and the climatostratigraphic nature of
391 isotope stages and substages. *Quaternary Science Reviews* 111:94–106.

392

393

394 **Figure Legends**

395



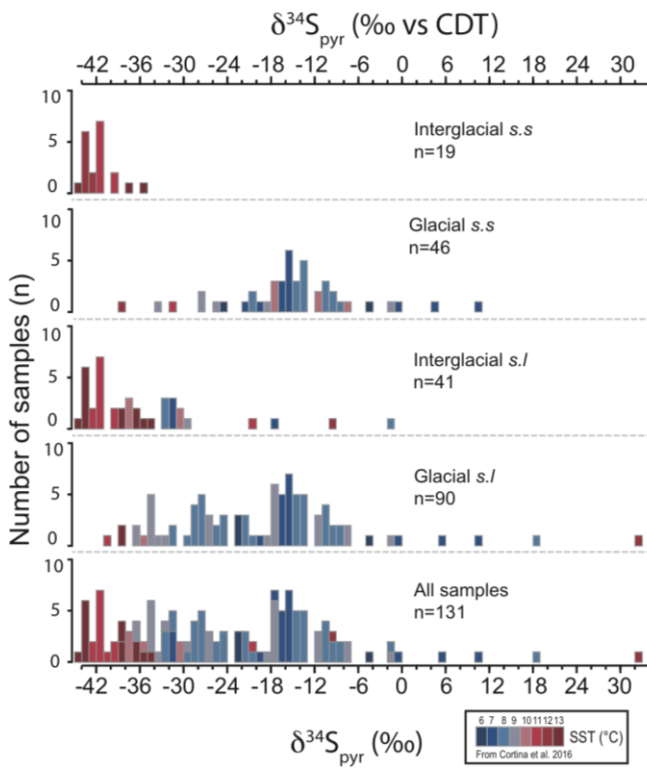
396

397 **Figure 1:** Map of the Gulf of Lion with the position of the PRGL1-4 core (42.690N; 3.838E).

398 The bold grey line highlights the present shoreline position and the contours reflect modern water

399 depths. The bold blue line corresponds to the shoreline position during the last-glacial period

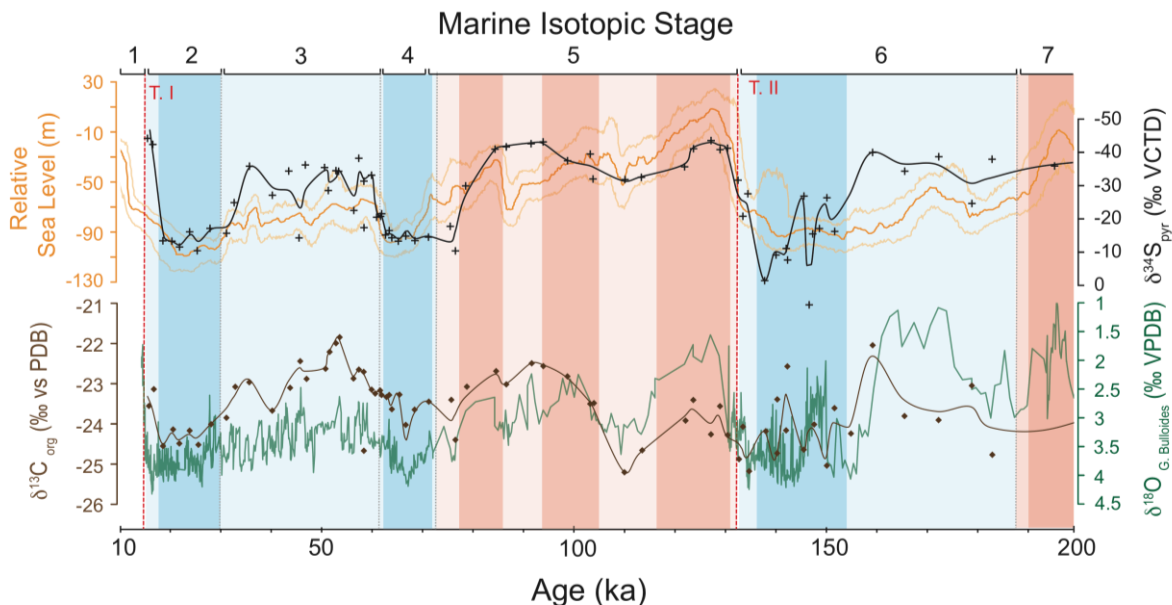
400 (low sea level).



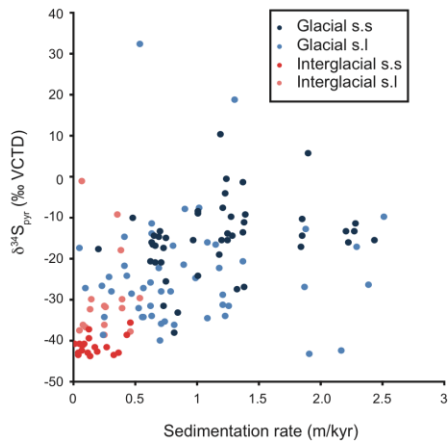
401

402 **Figure 2:** Histogram of pyrite $\delta^{34}\text{S}$ (this study) as a function of glacial/interglacial periods, color-

403 coded by temperature obtained from the relative composition of C₃₇ unsaturated alkenones (18,
 404 19). *Sensu stricto* (s.s.) refers to the warm substages of the interglacials and cold substages during
 405 glacials. The *sensu lato* (s.l.) includes all the data within interglacial or glacial periods.



406
 407 **Figure 3:** Glacial-interglacial geochemical records. $\delta^{34}\text{S}_{\text{pyr}}$ (black crosses; black line representing
 408 LOESS regression, this study), $\delta^{13}\text{C}_{\text{org}}$ (brown diamonds and brown line (LOESS regression), this
 409 study), reconstructed sea levels (orange) from the Red Sea, and $\delta^{18}\text{O}_{\text{G. Bulloides}}$ (green) for the last 6
 410 Marine isotopic stages (10 to 200 kyr). Relative Sea Level (orange line) superimposed with 95%
 411 of probability interval (light orange lines) from ref. 43 and $\delta^{18}\text{O}_{\text{G. Bulloides}}$ from ref. 17, 21. Blue
 412 vertical bands represent the glacial times with corresponding cold substages (i.e. *sensu-stricto*) in
 413 darker blue. Red bands correspond to interglacials periods with warm substages (i.e. *sensu-*
 414 *stricto*) highlighted in dark pink. Vertical pink dashed lines reflect glacial termination (T.) times
 415 according to ref. 44; vertical black dashed lines reflect scheme of marine stages according to ref.
 416 45.



417
 418 **Figure 4:** The relationship between sedimentation rate (m kyr^{-1}) and $\delta^{34}\text{S}_{\text{pyr}}$. Sedimentation rates
 419 are calculated using the linear relationship between depth in borehole and the update age model
 420 derived from ref. 17. Light / dark blues circles correspond to cold substages (i.e. respectively
 421 sensu-lato and *sensu-stricto*) whereas light / dark red circles refer to warm substages (i.e.
 422 respectively sensu-lato and *sensu-stricto*).
 423